Chinese Chemical Letters 35 (2024) 109525

Contents lists available at ScienceDirect

Chinese Chemical Letters

journal homepage: www.elsevier.com/locate/cclet

Subsurface carbon modification of Ni-Ga for improved selectivity in acetylene hydrogenation reaction

Shaoming Dong[a,b], Yiming Niu[a,b,*], Yinghui Pu[a,b], Yongzhao Wang[a,b], Bingsen Zhang[a,b,*]

[a] Shenyang National Laboratory for Materials Science, Institute of Metal Research, Chinese Academy of Sciences, Shenyang 110016, China
[b] School of Materials Science and Engineering, University of Science and Technology of China, Shenyang 110016, China

ARTICLE INFO

Article history:
Received 10 December 2023
Revised 1 January 2024
Accepted 11 January 2024
Available online 20 January 2024

Keywords:
Subsurface structure
Interstitial atom
Carbide
Hydrogenation reaction
Nickel alloy

ABSTRACT

Control of subsurface interstitial atoms in transition metals is an effective approach to modulate selectivity in hydrogenation reactions. In this study, nickel was alloyed with gallium to form Ni_3Ga, thereby regulating the octahedral interstitial sites. Subsequently, carbon atoms were introduced into the Ni_3Ga (forming $Ni_3GaC_{0.5}$) *via* thermal treatment in an acetylene atmosphere, leading to a significant enhancement in selectivity for acetylene hydrogenation reaction. The X-ray diffraction and transmission electron microscopy results demonstrate an increase in the lattice parameter due to the incorporation of carbon atoms and the uniform distribution of carbon in $Ni_3GaC_{0.5}$ nanoparticles. The obtained $Ni_3GaC_{0.5}$/oCNT catalyst exhibits significantly improved selectivity in acetylene hydrogenation reaction, with approximately 82% ethylene selectivity at 98% conversion. Furthermore, it maintains good selectivity at various hydrogen-to-alkyne ratios and displays good stability during long-term operation. The introduction of carbon suppresses the formation of the subsurface hydrogen structure under reaction conditions. Additionally, the charge transfer between carbon and nickel results in the electron deficiency of nickel, effectively inhibiting the over-hydrogenation pathway and enhancing the selectivity. These results provide insights for the design of non-precious metal catalysts in selective hydrogenation reactions.

Ethylene is one of the fundamental raw materials and serves as the precursor for chemical intermediates such as polyethylene, ethylbenzene, ethylene oxide, and dichloroethane [1]. Generally, ethylene is obtained through the cracking of naphtha, which typically co-produces a trace amount of acetylene (0.5% to 3.0%) [2]. Acetylene can react with the Ziegler-Natta catalyst in the subsequent polymerization process, which is the primary use of ethylene, leading to catalyst deactivation and product degradation [3]. The acetylene content in ethylene feed should be reduced to below 5 ppm prior to polymerization [4,5]. Typically, the trace acetylene is removed from ethylene through selective hydrogenation using supported metal catalysts in the industry [6–9]. Acetylene hydrogenation catalysts are required to efficiently remove acetylene in the presence of excess ethylene. Therefore, the catalyst must exhibit both high activity and high selectivity to prevent the over-hydrogenation of ethylene, which could lead to unnecessary ethylene consumption and potentially reaction runaway due to this highly exothermic process. Additionally, the formation of carbon deposition, which could result in catalyst deactivation, should be avoided during the reaction.

The catalytic performance in acetylene hydrogenation is primarily determined by the catalyst structure. Under reaction conditions, light elements can incorporate into the metal interstitial sites and form various subsurface structures. These distinct interstitial atoms can influence the structure of active sites or directly participate in the reactions, thereby affecting the reaction mechanism and catalytic performance [10–14]. Subsurface interstitial hydrogen structures can be generated and can affect the catalysis during hydrogenation reactions. For instance, Maeland *et al.* identified two types of Pd hydrides with face-centered cubic structures: α-PdH_x and β-PdH_x, under low and high hydrogen content atmospheres, respectively [15]. Subsequent studies revealed that the β-PdH_x structure exhibited higher catalytic activity but lower selectivity compared to α-PdH_x in acetylene hydrogenation reactions [16,17]. It was found that carbon atom can also be introduced into the subsurface interstitial sites and modulate the catalytic performance of Pd during catalysis [16]. Teschner *et al.* demonstrated that subsurface carbon can inhibit the hydrogen atom introduction and enhance the selectivity during alkyne hydrogenation reactions [18]. Theoretical calculations have shown that subsurface

* Corresponding authors.
E-mail addresses: ymniu14b@imr.ac.cn (Y. Niu), bszhang@imr.ac.cn (B. Zhang).

https://doi.org/10.1016/j.cclet.2024.109525
1001-8417/

carbon atoms can influence the adsorption strength of acetylene and ethylene on the Pd surface, thereby improving ethylene selectivity [19].

Based on the demand for high activity and selectivity in acetylene hydrogenation reaction, supported palladium-based catalysts were generally adopted in industry. However, due to the limited reserves and high cost of palladium, replacing it with non-precious metals has drawn much attention. The non-precious metal nickel is highly active and has widely served as hydrogenation catalysts [20–23]. However, Ni catalysts often result in the over-hydrogenation of ethylene and significant deactivation in the acetylene hydrogenation reaction. This is attributed to the strong bonding with intermediates and the formation of subsurface hydrogen structures during catalysis [24–26]. Therefore, modulating the surface/subsurface structure of Ni has been investigated to improve the catalytic performance in these reactions [27,28]. Ni shares a similar electronic structure and exhibits dynamic subsurface behavior comparable to Pd under reaction conditions [18,29]. Controlling subsurface atoms can serve as an effective approach to improving its selectivity. However, introducing carbon into the interstitial sites of Ni is quite challenging and can lead to phase transitions, surface encapsulation, and even carbon layer growth. In our previous studies, we addressed this issue by introducing Zn to form the Ni_3Zn alloy, thereby expanding its octahedral interstitial site and successfully incorporating carbon atoms under an acetylene atmosphere at low temperatures. The obtained $Ni_3ZnC_{0.7}$ catalyst exhibits superior selectivity and stability in selective hydrogenation reactions [30,31].

Herein, our research seeks to further understand and enhance the selectivity of Ni-based catalysts for acetylene hydrogenation by manipulating the subsurface structure. Through alloying nickel with gallium, we prepared the supported Ni_3Ga structure, which facilitates the incorporation of carbon atoms into its octahedral interstitial sites, resulting in the formation of $Ni_3GaC_{0.5}$ catalysts. The successful alloying and carbon introduction were confirmed by X-ray diffraction (XRD) and transmission electron microscopy (TEM). The catalytic performance of the obtained Ni-based catalysts was further evaluated under various hydrogenation conditions, focusing on their selectivity and stability. Moreover, the changes in the nickel electronic structure after carbon incorporation were investigated, aiming to establish a correlation between structural evolution and catalytic performance.

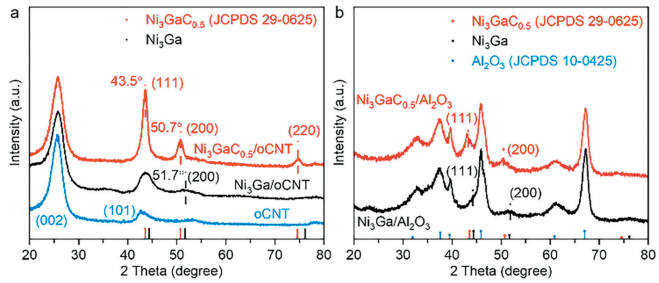

Fig. 1. XRD patterns of Ni_3Ga and $Ni_3GaC_{0.5}$ supported on (a) oCNT and (b) Al_2O_3, respectively.

The supported alloy and interstitial carbide catalysts were prepared through an impregnation method followed by hydrogen reduction and acetylene treatment. XRD was employed to identify the phase structure of Ni_3Ga and $Ni_3GaC_{0.5}$. As shown in Fig. 1 and Fig. S1 (Supporting information), a prominent diffraction peak at 51.7° was observed in Ni_3Ga/oCNT, Ni_3Ga/Al_2O_3, and Ni_3Ga/SiN catalysts, corresponding to the (200) crystal plane of the Ni_3Ga intermetallic compound with a face-centered cubic (FCC) structure. The XRD results confirm the successful fabrication of the Ni_3Ga alloy structure through impregnation and reduction on different supports. After the acetylene treatment, the obtained catalysts demonstrated a slight shift of the diffraction peaks relative to the Ni_3Ga phase, specifically observed at 43.5°, 50.7°, and 74.6°. These peaks, corresponding to the (111), (200), and (220) crystal planes of $Ni_3GaC_{0.5}$, suggest an expanded lattice spacing. These results indicate the successful incorporation of carbon atoms into the octahedral interstitial sites of Ni_3Ga following acetylene treatment. It is worth noting that the same method was successfully employed to prepare $Ni_3GaC_{0.5}$ catalysts with interstitial carbide structure on different supports.

Subsequently, the microstructure of the obtained catalysts was systematically identified using TEM techniques, which are a powerful tool for characterizing the structure of supported catalysts [32,33]. Figs. 2a and b display the typical TEM images of the Ni_3Ga/oCNT and $Ni_3GaC_{0.5}$/oCNT catalysts, accompanied by histograms that illustrate the particle size distribution (PSD). Both Ni_3Ga and $Ni_3GaC_{0.5}$ nanoparticles (NPs) exhibit a uniform dis-

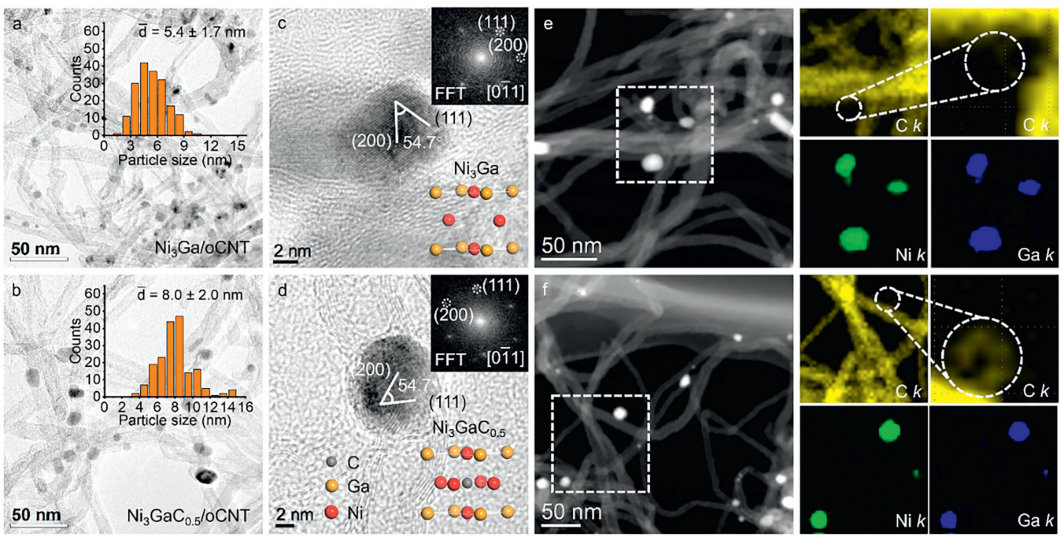

Fig. 2. TEM and HRTEM images of (a, c) Ni_3Ga/oCNT and (b, d) $Ni_3GaC_{0.5}$/oCNT. The top-right insets are the corresponding PSD histograms and FFTs. HAADF-STEM images of (e) Ni_3Ga/oCNT and (f) $Ni_3GaC_{0.5}$/oCNT with the corresponding EDX elemental maps of C (yellow), Ni (green), and Ga (blue).

tribution on the oCNT support. The PSD analysis indicated a size range of 1.0–11.0 nm for the Ni_3Ga NPs, with an average size of 5.4 ± 1.7 nm. After acetylene treatment, the Ni_3Ga NPs underwent a structural transformation; carbon atoms occupied the octahedral interstitial sites within the Ni_3Ga alloy, resulting in the formation of the $Ni_3GaC_{0.5}$ structure. This process leads to a significant increase in particle size, ranging from 2.0 nm to 15.0 nm with an average of 8.0 ± 2.0 nm. Moreover, a comprehensive microstructural analysis of both catalysts was conducted using high-resolution (HR) TEM. As shown in Fig. 2c and Fig. S2 (Supporting information), HRTEM results reveal that the lattice spacings of the NP are 0.204 nm and 0.177 nm, with an angle of 54.7°. These values correspond to the (111) and (200) crystal planes of Ni_3Ga, respectively. After the catalyst was treated with an acetylene atmosphere to introduce carbon atoms, lattices with the same angle of 54.7° was observed in the HRTEM image, showing increased spacings of 0.208 nm and 0.180 nm (Fig. 2d and Fig. S2), corresponding to the (111) and (200) crystal planes of $Ni_3GaC_{0.5}$, respectively. These results, consistent with the crystal structure of Ni_3Ga and $Ni_3GaC_{0.5}$, confirm that carbon atoms were introduced into the Ni_3Ga interstitial sites through acetylene treatment.

Further characterization was carried out using energy-dispersive X-ray spectroscopy (EDX) elemental mapping to ascertain the composition and distribution of elements within the catalysts. Fig. 2e and Fig. S3 (Supporting information) display the high-angle annular dark-field scanning TEM (HAADF-STEM) images of the Ni_3Ga/oCNT catalyst, where the K-edge signals of Ni and Ga are homogeneously distributed on the oCNT support, and no carbon signals are detected within the NPs, indicating a bimetallic alloy structure. Following acetylene treatment, as shown in Fig. 2f and Fig. S4 (Supporting information), the $Ni_3GaC_{0.5}$/oCNT catalyst exhibits the presence of Ni, Ga, and C within the NPs, demonstrating a homogeneous distribution of all three elements and the successful formation of the interstitial carbide structure.

The catalytic performance of these catalysts in the selective hydrogenation of acetylene was subsequently investigated. Fig. S5 (Supporting information) displays the performance of the $Ni_3GaC_{0.5}$/oCNT and Ni_3Ga/oCNT catalysts, highlighting their acetylene conversion and ethylene selectivity across a temperature range of 50–180 °C. The $Ni_3GaC_{0.5}$/oCNT catalyst displayed an enhancement in acetylene conversion from 3% to 100% as the temperature was raised, while the ethylene selectivity impressively remained above 70% throughout this range. In contrast, the Ni_3Ga/oCNT catalyst demonstrated a sharp decrease in ethylene selectivity, falling to approximately −220%, as the acetylene conversion increased. The negative value of ethylene selectivity is due to the simultaneous hydrogenation of the large amount of ethylene to ethane in the feed gas.

The activity and selectivity of the catalysts under various hydrogen to acetylene ratios are depicted in Figs. 3a and b. The results demonstrated that the activity of both catalysts increased as the hydrogen ratio increased. The $Ni_3GaC_{0.5}$/oCNT catalyst exhibited high selectivity across a wide range of H_2/C_2H_2 ratios, indicating its stability under fluctuating hydrogen conditions. Conversely, the Ni_3Ga/oCNT catalyst displayed a significant decrease in ethylene selectivity with increasing hydrogen concentration, accompanied by a rapid increase in selectivity towards the over-hydrogenation product ethane. The results indicate that variations in H_2 concentration significantly influence the hydrogenation reaction on the surface of bimetallic alloy catalysts.

Furthermore, the $Ni_3GaC_{0.5}$/oCNT catalyst illustrates the remarkable ethylene selectivity, reaching up to 82% with nearly complete acetylene conversion (Fig. S6 in Supporting informaiton). The catalyst also showed selectivity of 7% for the full hydrogenation product ethane and 11% for the polymerization products C_4. On the other hand, the Ni_3Ga/oCNT catalyst exhibited extremely poor

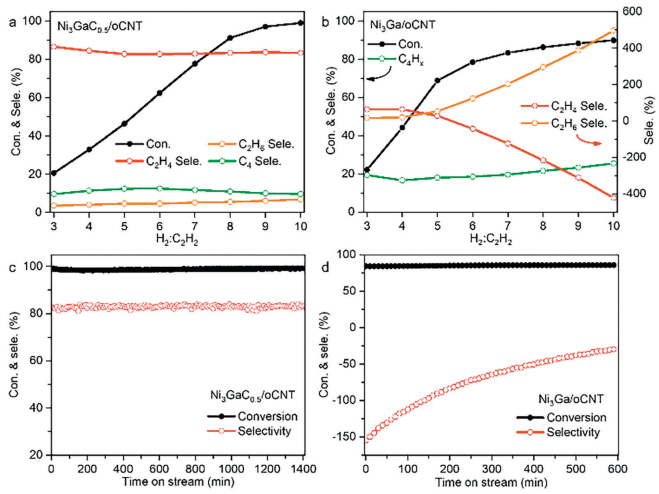

Fig. 3. Conversion and selectivity of (a) $Ni_3GaC_{0.5}$/oCNT and (b) Ni_3Ga/oCNT catalysts under various H_2 to C_2H_2 ratios in acetylene hydrogenation reaction. Stability test of (c) $Ni_3GaC_{0.5}$/oCNT and (d) Ni_3Ga/oCNT, respectively. Reaction conditions: 0.5 vol% C_2H_2, 20.0 vol% C_2H_4, 1.5–5.0 vol% H_2, helium as balance.

ethylene selectivity, reflected by a value of −497% at 92% acetylene conversion, primarily due to the over-hydrogenation of ethylene to ethane, which resulted in an ethane selectivity as high as 563%. Additionally, the interstitial carbide catalyst displayed approximately 23% lower selectivity for C_4 compared to the bimetallic alloy catalyst, indicating an inhibition of the reaction pathway for polymerization products. The long-term stability test of the $Ni_3GaC_{0.5}$/oCNT catalyst, as illustrated in Fig. 3c, underscored its exceptional stability with acetylene conversion (98%) and ethylene selectivity (83%) remaining virtually unchanged over a 23-h test period, indicating no significant deactivation. In contrast, the Ni_3Ga/oCNT catalyst, maintained consistent acetylene conversion but showed an increase in ethylene selectivity from −154% to approximately −30% (Fig. 3d). This suggests a potential decrease in the conversion rate of feed ethylene, hinting at gradual catalyst deactivation over time. Such improved stability of the $Ni_3GaC_{0.5}$/oCNT catalyst is attributed to the interstitial carbon structure, which inhibits the formation of carbonaceous deposits on the catalyst surface, in accordance with previous studies [30].

The electronic structure of the catalytic active sites is crucial for the selectivity and efficiency of hydrogenation reactions, as it governs the adsorption thermodynamics and kinetic barriers for reactants and products [34]. X-ray photoelectron spectroscopy (XPS) was employed to probe the electronic structure of Ni_3Ga/oCNT and $Ni_3GaC_{0.5}$/oCNT catalysts (Fig. 4). The high-resolution XPS spectra (Fig. 4b) demonstrate Ni^{2+} and Ni^0 states with binding energies for Ni^{2+} $2p_{1/2}$ and Ni^{2+} $2p_{3/2}$ at 873.1 and 855.4 eV, respectively, alongside Ni^0 $2p_{1/2}$ and Ni^0 $2p_{3/2}$ peaks at 869.8 and 852.7 eV. The satellite peaks associated with Ni, manifested in the green region of the spectrum, suggest a significant oxidation of Ni within the alloy under the *ex-situ* characterizations, primarily leading to the observation of Ni^{2+} species [35].

In the case of the $Ni_3GaC_{0.5}$/oCNT catalyst, the binding energies for Ni^0 $2p_{1/2}$ and Ni^0 $2p_{3/2}$ are observed at 870.2 and 853.1 eV, respectively. These values represent a notable shift by approximately 0.4 eV to higher binding energies relative to the Ni_3Ga/oCNT catalyst. Such a shift can be rationalized by the increased electronegativity of carbon (2.5) in comparison to nickel (1.9), which suggests the formation of an interstitial carbide that alters the electronic structure of Ni, leading to the electron deficiency of Ni. In addition, a marginal elevation in the binding energy of the Ga^0 $2p_{3/2}$ peak for the $Ni_3GaC_{0.5}$ catalyst, as detailed in Fig. S7 (Supporting

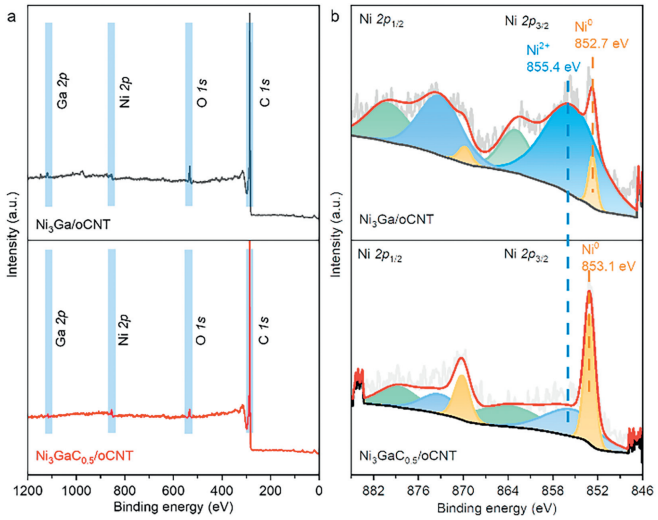

Fig. 4. (a) XPS survey and (b) Ni 2p spectra of Ni_3Ga/oCNT and $Ni_3GaC_{0.5}$/oCNT catalyst, respectively.

information), provides further evidence of charge transfer between Ga and C atoms, indicative of the formed interstitial carbide structure.

Indeed, the XPS results coupled with the electronic structure analysis suggest that the electron transfer from Ni active sites to the interstitial carbons is the underlying reason for the observed performance difference between the Ni_3Ga/oCNT and $Ni_3GaC_{0.5}$/oCNT catalysts. This electron transfer leads to a more electron-deficient state of Ni, which weakens the adsorption strength of reaction intermediates on the catalyst surface, thus enhancing the selectivity [36]. Furthermore, it has been shown that subsurface hydrogen in Ni-based catalysts is more reactive compared to surface hydrogen during selective hydrogenation processes. The formation of interstitial carbide structures can effectively block the formation of subsurface hydrogen and its participation in the reaction, preventing over-hydrogenation [18].

In this study, the Ni_3Ga and $Ni_3GaC_{0.5}$ catalysts on different supports were successfully prepared using the impregnation method. TEM analysis confirmed the uniform distribution of single-crystal NPs on the oCNT support for both catalysts. EDX elemental mapping further validated the homogeneous distribution of elements within the catalysts. The XPS results showed that the incorporation of interstitial carbon atoms into the $Ni_3GaC_{0.5}$ catalysts imparts a distinctive electronic structure to the Ni active site, which is conducive to the desorption of intermediates in selective hydrogenation reactions. The formation of subsurface interstitial carbon and the resultant electron-deficient state of Ni are crucial for improving the performance of the acetylene selective hydrogenation reaction, leading to enhanced ethylene selectivity and stability. The findings of this study offer valuable insights into the structure-performance relationship of transition metal catalysts with interstitial modifications, highlighting the importance of the electronic structure modulation of the Ni active site by the presence of carbon atoms in the $Ni_3GaC_{0.5}$/oCNT catalyst in achieving efficient selective hydrogenation of acetylene. These insights contribute to the design of novel non-precious metal catalysts with superior catalytic properties.

Declaration of competing interest

The authors declare that they have no known competing financial interests or personal relationships that could have appeared to influence the work reported in this paper.

Acknowledgments

We gratefully acknowledge the financial support provided by the National Natural Science Foundation of China (Nos. 22002173, 22072164, 52161145403), Natural Science Foundation of Liaoning Province (No. 2022-MS-004), China Postdoctoral Science Foundation (No. 2020M680999), LiaoNing Revitalization Talents Program (No. XLYC1807175), and the foundations of Shenyang National Laboratory for Materials Science.

Supplementary materials

Supplementary material associated with this article can be found, in the online version, at doi:10.1016/j.cclet.2024.109525.

References

[1] K. Lian, Y. Zhu, W. Li, S. Dai, C. Chen, Macromolecules 50 (2017) 6074–6080.
[2] Y. Liu, B. Wang, Q. Fu, et al., Angew. Chem. Int. Ed. 60 (2021) 22522–22528.
[3] H. Bazzazzadegan, M. Kazemeini, A.M. Rashidi, Appl. Catal. A: Gen. 399 (2011) 184–190.
[4] D.S. Sholl, R.P. Lively, Nature 532 (2016) 435–437.
[5] Y. Chai, X. Han, W. Li, et al., Science 368 (2020) 1002–1006.
[6] C. Crespos, H.F. Busnengo, W. Dong, A. Salin, J. Chem. Phys. 114 (2001) 10954–10962.
[7] S. Komhom, O. Mekasuwandumrong, P. Praserthdam, J. Panpranot, Catal. Commun. 10 (2008) 86–91.
[8] H.Y. Fang, D.S. Wang, X.W. Liu, D.R. Zhu, Y.D. Li, Acta Phys. Chim. Sin. 39 (2023) 2305030.
[9] M.R. Wang, Y.X. Yue, Y. Wang, et al., J. Energy Chem. 69 (2022) 541–554.
[10] T. Chen, C. Foo, S.C. Edman Tsang, Chem. Sci. 12 (2020) 517–532.
[11] J. Li, L.Y. Cai, X.S. Liang, et al., J. Energy Chem. 79 (2023) 550–558.
[12] D. Chen, R. Lu, R. Yu, et al., Nano-Micro Lett. 15 (2023) 168.
[13] L. Ma, X. Gao, X. Liu, et al., Chin. Chem. Lett. 34 (2023) 107735.
[14] G. Zhang, A. Wang, L. Niu, et al., Adv. Energy Mater. 12 (2022) 2103511.
[15] A.J. Maeland, T. Jr, J. Phys. Chem. 65 (1961) 1270–1272.
[16] A. Borodziński, G.C. Bond, Catal. Rev. 48 (2006) 91–144.
[17] A. Borodziński, A. Janko, React. Kinet. Catal. Lett. 7 (1977) 163–169.
[18] D. Teschner, J. Borsodi, A. Wootsch, et al., Science 320 (2008) 86–89.
[19] F. Studt, F. Abild-Pedersen, T. Bligaard, et al., Angew. Chem. Int. Ed. 47 (2008) 9299–9302.
[20] A. Jalal, A. Uzun, Appl. Catal. A: Gen. 562 (2018) 321–326.
[21] Y. Zhu, M. Yang, Z. Zhang, et al., Chin. Chem. Lett. 33 (2022) 2069–2072.
[22] X. Huang, Y. Ma, L. Zhi, Acta Phys. Chim. Sin. (2020) 2011050.
[23] Y.N. Shang, X.G. Duan, S.B. Wang, et al., Chin. Chem. Lett. 33 (2022) 663–673.
[24] Z. Li, J. Zhang, J. Tian, et al., Chem. Eng. J. 450 (2022) 138244.
[25] C.M. Kruppe, J.D. Krooswyk, M. Trenary, ACS Catal. 7 (2017) 8042–8049.
[26] L. Zhang, Z. Chen, Z. Liu, et al., Nat. Commun. 12 (2021) 6574.
[27] J. Osswald, K. Kovnir, M. Armbruster, et al., J. Catal. 258 (2008) 219–227.
[28] Y. Liu, X. Liu, Q. Feng, et al., Adv. Mater. 28 (2016) 4747–4754.
[29] S.T. Ceyer, Acc. Chem. Res. 34 (2001) 737–744.
[30] Y.M. Niu, X. Huang, Y.Z. Wang, et al., Nat. Commun. 11 (2020) 3324.
[31] S.M. Dong, Y.H. Pu, Y.M. Niu, et al., Acta Phys. Chim. Sin. 39 (2023) 2301012.
[32] D.S. Su, B. Zhang, R. Schlogl, Chem. Rev. 115 (2015) 2818–2882.
[33] Y.M. Niu, B.S. Zhang, Curr. Opin. Green Sustain. Chem. 22 (2020) 22–28.
[34] S. Furukawa, T. Komatsu, ACS Catal. 7 (2017) 735–765.
[35] J.P. Boitiaux, J. Cosyns, E. Robert, Appl. Catal. 49 (1989) 235–246.
[36] X. Ge, M. Dou, Y. Cao, et al., Nat. Commun. 13 (2022) 5534.